THE JOURNAL OF PHYSICAL CHEMISTRY Letters

Perspective

pubs.acs.org/JPCL

Plasmon-Enhanced Upconversion

Di M. Wu,[†] Aitzol García-Etxarri,[‡] Alberto Salleo,[‡] and Jennifer A. Dionne*[,‡]

[†]Department of Chemistry and [‡]Department of Materials Science and Engineering, Stanford University, Stanford, California 94305, United States

ABSTRACT: Upconversion, the conversion of photons from lower to higher energies, is a process that promises applications ranging from high-efficiency photovoltaic and photocatalytic cells to background-free bioimaging and therapeutic probes. Existing upconverting materials, however, remain too inefficient for viable implementation. In this Perspective, we describe the significant improvements in upconversion efficiency that can be achieved using plasmon resonances. As collective oscillations of free electrons, plasmon resonances can be used to enhance both the incident electromagnetic field intensity and the radiative emission rates. To date, this approach has shown upconversion enhancements up to 450×. We discuss both theoretical underpinnings and experimental demonstrations of plasmon-enhanced upconversion, examining the roles of upconverter quantum yield, plasmonic geometry, and plasmon spectral overlap. We also discuss nonoptical consequences of including metal nanostructures near upconverting emitters. The rapidly expanding field of plasmon-enhanced upconversion provides novel fundamental insight into nanoscale light−matter interactions while improving prospects for technological relevance.

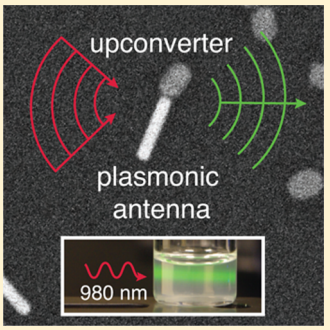

Luminescent materials typically emit photons of lower energy than those absorbed. In contrast, upconverting materials absorb low-energy photons and emit photons of higher energy, a property that can be applied in many exciting ways. Upconverters can act as protein-sized luminescent probes for single-molecule microscopy[1] and enable low-background bioimaging using near-infrared light that penetrates deeply into tissue.[2] They can also extend the optical working range of devices such as photoswitchable selective reflectors[3] and soft actuators[4] into the red and infrared. Further, upconverting materials could enable solar cells without transmission losses that use nearly the full solar spectrum to generate photocurrent[5,6] or security inks for printing patterns visible only in certain power and spectral conditions.[7]

Along with considerations including spectral alignment, bandwidth, size, phase, and stability, a major limitation in implementing upconverters is the low efficiency of existing materials. Extensive work has been performed in modifying upconverting materials to improve efficiency, addressing properties including the host medium, dopants, and surface chemistry.[8−10] In concert with these approaches, engineering the electromagnetic environment experienced by upconverting materials using photonic crystals,[11,12] antenna dyes,[13] quantum dots,[14] and plasmonic structures allows for further increases in performance. We devote this review to plasmon-enhanced upconversion, a strategy that has shown upconversion enhancements of up to 450×.

The goal of plasmon-enhanced upconversion is to improve both absorption and emission processes by tailoring the electric and magnetic fields at the position of an upconverting emitter. This improvement is accomplished using the high-frequency electromagnetic resonances of electrons in conducting materials. While this principle may appear straightforward, complexities arise from the multistep nature of the upconversion process. Despite encouraging progress, much work remains toward realizing comprehensive design principles for optimal upconversion enhancement. In this Perspective, we first introduce commonly studied upconverting materials and then describe the theoretical framework for plasmon-enhanced upconversion. Next, we highlight recent experimental work exploring the roles of plasmonic geometry and spectral overlap. Finally, after a discussion of nonoptical effects of plasmon-modified upconversion, we conclude the review with open questions and emerging opportunities in the field.

The goal of plasmon-enhanced upconversion is to improve both absorption and emission processes by tailoring the electric and magnetic fields at the position of an upconverting emitter.

Upconverting Materials and Mechanisms. Energy-transfer upconversion occurs through the population of and subsequent energy transfer between real intermediate states. The excitation pathway through these intermediate states differentiates upconversion from other nonlinear optical processes such as multiple harmonic generation or multiple photon absorption. In particular, because photons interacting with upconverting materials are absorbed into these real states rather than virtual

Received: September 8, 2014
Accepted: October 30, 2014
Published: October 30, 2014

   dx.doi.org/10.1021/jz5019042 | J. Phys. Chem. Lett. 2014, 5, 4020−4031

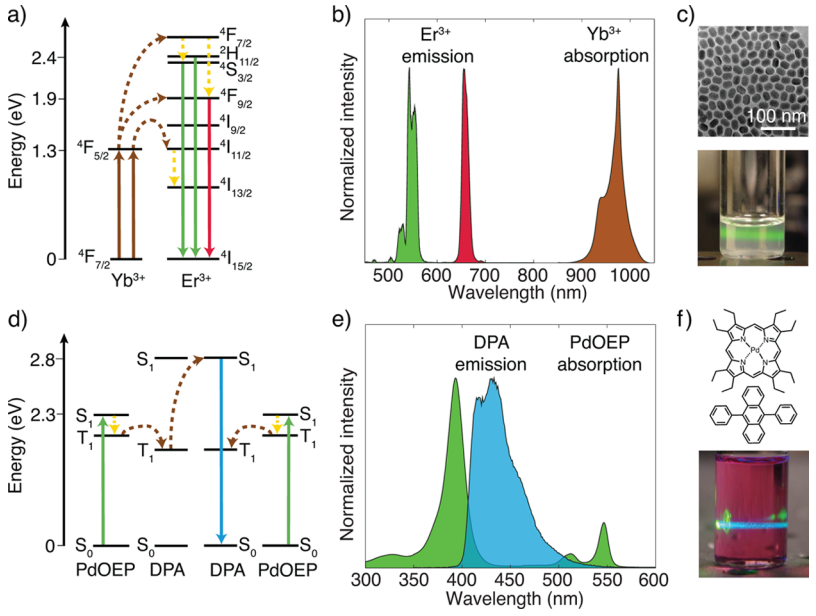

Figure 1. (a) Energy diagram and simplified mechanism for energy-transfer upconversion between Yb^{3+} and Er^{3+}. Solid arrows denote absorption and emission, dashed brown arrows denote interspecies energy transfer, and dashed yellow arrows denote nonradiative relaxation. (b) Absorption and emission spectra for the ions depicted in (a). (c) Transmission electron micrograph of $NaYF_4$/18%Yb^{3+}, 2% Er^{3+} nanoparticles; photograph of upconversion emission from the nanoparticle colloid upon excitation at 980 nm. (d) Energy diagram and mechanism for energy-transfer upconversion in palladium octylethylporphyrin (PdOEP) and diphenylanthracene (DPA). Arrows follow the same notation as those in (a). (e) Absorption and emission spectra for the molecules depicted in (d). (f) Molecular structure of PdOEP and DPA; photograph of upconversion emission from a solution of PdOEP and DPA upon excitation at 532 nm.

states, upconversion can exhibit efficiencies up to 11 orders of magnitude higher than second-harmonic generation.[15]

Two commonly studied upconverting systems are lanthanide ions embedded in dielectric matrixes and pairs of molecular dyes. In lanthanide ions, the intermediate states that lead to upconverted emission are 4f orbital energy levels. These 4f orbitals are shielded from the outside chemical environment by outer-lying 6s and 6p orbitals and do not participate in bonding to a significant degree. The f orbital states therefore effectively maintain their atomic character, and electric dipole transitions between them remain parity-forbidden. Nonradiative decay is suppressed by embedding the ions in a host lattice with low-energy phonon modes. As a result, the excited states are metastable, enabling long-lived intermediate states that then allow for sequential energy transfers.

Figure 1a illustrates the mechanism leading to upconversion in the sensitizer−emitter pair Yb^{3+} and Er^{3+}. Absorption of light at 980 nm in Yb^{3+} is followed by energy transfer to the $^4I_{11/2}$ energy level in Er^{3+}. A second absorption and energy-transfer event populates a higher-energy state, which, after nonradiative relaxation, leads to emission in the visible with strong peaks at 540 and 660 nm (as seen in Figure 1b). This pair of ions exhibits the highest upconversion efficiency from 980 nm to the visible, with absolute efficiencies depending on the host matrix and excitation power. Note that the upconversion quantum efficiency (the ratio of photons emitted to photons absorbed) has a maximum theoretical value of 50% for a two-photon upconversion process. In bulk hexagonal (β) $NaYF_4$/18% Yb^{3+}, 2% Er^{3+}, upconversion efficiencies of 4% have been reported for upconversion from 980 to 540 nm.[16] In nanostructures of the same material, the efficiency decreases with decreasing size as surface states quench emission.[17,18] The reported upconversion efficiency of 30 nm $NaYF_4$/20% Yb^{3+}, 2% Er^{3+} nanoparticles ranges from 0.1 up to 0.3% with the introduction of a passivating shell.[17] For many applications, the small size and solution processability of upconverting nanoparticles make them attractive despite their decreased efficiency. Strategies to enhance upconversion emission from nanoparticles are therefore of particular interest.

Figure 1c shows a colloid of upconverting nanoparticles in cyclohexane, excited at 980 nm and emitting green light. A micrograph inset shows the nanoparticle morphology. Synthetic progress has led to outstanding control over nanoparticle shape, size, phase, and monodispersity. Major advantages of lanthanide upconverters include the ability to upconvert over large wavelength ranges (from infrared absorption to ultraviolet emission; for example, see ref 19), absence of blinking or photobleaching,[20] environmental stability, and relatively low toxicity.[21] Limitations include low tunability of absorption and emission and low efficiency due to the forbidden nature of the optical transitions.

A second type of upconverter are pairs of organic molecules that populate a singlet excited state through triplet energy transfer. There are many combinations of dyes and polymers that upconvert, allowing for tunable absorption and emission bands throughout the visible spectrum.[22] In Figure 1, we show the energy level diagram and absorption/emission characteristics for the well-studied upconverting molecular pair palladium octylethylporphyrin (PdOEP) and diphenylanthracene (DPA). The mechanism leading to upconversion is shown in Figure 1d. First, a sensitizer dye absorbs low-energy light to a singlet excited state and then undergoes rapid intersystem crossing to a triplet excited state. Triplet relaxation to the ground state is spin-forbidden, and these states are analogous to the metastable intermediate states in lanthanide ions. Energy transfer from this triplet state to a lower-lying triplet state in an emitter molecule generates a population of long-lived intermediates. Finally, when two excited-state emitter mole-

dx.doi.org/10.1021/jz5019042 | J. Phys. Chem. Lett. 2014, 5, 4020−4031

cules encounter each other at a short distance, energy transfer through triplet−triplet annihilation populates a singlet state that then undergoes rapid radiative decay, emitting light blue-shifted from that absorbed.

The normalized absorption and emission spectra for PdOEP and DPA, respectively, are shown in Figure 1e. Excitation at 532 nm leads to upconverted emission at 440 nm. Note that PdOEP also has a Soret peak absorption at 390 nm that does not participate in upconversion. Figure 1f shows a solution of 0.02 mM PdOEP and 15 mM DPA in toluene, excited at 532 nm and emitting blue light. The chemical structures of the molecules are inset. Major advantages of bimolecular upconverters include their higher upconversion efficiency (up to 16% reported in solution)[6,23] and larger absorption coefficient relative to the lanthanide ions (on the order of 10^{-16} cm^2 as compared to 10^{-20} cm^2)[24,25] and their tunable absorption and emission wavelengths using the large library of available dyes and synthetic techniques. Challenges include luminescence quenching by oxygen and decreased upconversion efficiency in the solid state due to reduced molecular mobility, which decreases energy transfer between molecules.[9]

Theoretical Foundations of Plasmon-Enhanced Upconversion. To externally enhance luminescence from a material, two approaches that one might take are to increase the incident illumination flux or to increase the radiative decay rate. Both can be done using plasmons, which are collective oscillations of free charges; a surface plasmon, in particular, is an oscillation at the interface between a material with free electrons (e.g., a metal or doped semiconductor) and a dielectric material (e.g., air or glass).[26] When light couples to a surface plasmon, it can become highly confined near the interface, leading to enhanced electromagnetic fields that result in increased absorption cross sections. In turn, these enhanced fields can modify the local density of optical states, leading to faster radiative decay rates.[27] Essentially, plasmonic structures act as optical nanoantennas, enabling improved reception and transmission of incident electromagnetic fields by the upconverter.[28]

There are three main ways in which a plasmonic nanoantenna can influence a nearby emitter. First, the antenna can locally concentrate the incident field and enhance absorption, improving reception. The antenna can also enhance emission by increasing the emitter's radiative decay rate, improving transmission. On the other hand, the antenna can also quench emission by increasing the nonradiative decay rate, decreasing transmission. The interplay of these three processes depends on spectral overlap between the resonances and absorption/emission frequencies, field overlap, polarization, antenna material, and pump power.[29] Noble metal nanoparticles, which have shape- and size-tunable plasmon resonances in the visible and near-infrared, are a well-studied type of optical nanoantenna. They can be colloidally synthesized or lithographically fabricated. Important antenna design considerations include antenna material/shape/size (controlling spectral overlap),[30] emitter position relative to the antenna (controlling field overlap),[31] and antenna orientation relative to the source polarization (controlling polarization).[32]

Plasmon resonances have been used to significantly enhance many processes, including Raman scattering,[33,34] infrared absorption,[35] and fluorescence,[31] with enhancements of 10^8−10^{15}, 10^4, and 10^3 reported for each process, respectively.[34,36−38] While the mechanism leading to upconversion has similarities with these processes, there are several features particular to plasmon-enhanced upconversion that merit careful consideration:

(1) Upconversion can result in large spectral shifts, with absorption separated from emission by more than 1 eV. Upconversion may therefore necessitate new strategies for maximizing spectral overlap between the plasmon resonance and the emitter absorption and emission frequencies.

(2) Upconversion is a multistep process involving long-lived intermediate states that each have competitive decay pathways. Plasmon resonances can increase the decay rate from these intermediate states, reducing the efficiency of upconversion. Furthermore, the populations of excited states leading to upconversion are interdependent; when the population of one state changes due to a change in decay rate, the others will also be modified.

(3) Upconversion depends strongly on input power. The power emitted by an upconverter has a nonlinear dependence on incident field intensity at low powers that becomes a linear process at high powers.[39,40] The effect of a plasmon resonance near an upconverting emitter is therefore expected to show a power dependence. The turning point from the low power regime to the high power regime depends on the transition rates of the excited-state manifolds, which, as noted before, can change in the presence of a metallic nanostructure.

In summary, a plasmonic nanostructure affords incident field intensity enhancements and enhanced radiative decay from emitting states that are expected to increase upconversion emission, but quantitative prediction of these effects requires knowledge of the specific transition rates of the upconverting material as well as the incident flux.

Thus far, theoretical studies of plasmon-enhanced upconversion have typically used full-field simulations to calculate the field enhancement and change in decay rates near an isolated plasmonic structure. These effects can then be input to a model that uses rate equations to describe the population of states in the upconverter at a given incident flux.[41] A simple rate equation model, based on a generic three-level upconverter, found a maximum enhancement of 3.5× for energy-transfer upconversion near a 400 nm diameter gold sphere.[42] A more specific approach studied the change in population of erbium's six lowest-energy excited states near a 200 nm gold sphere.[43,44] In that case, a 4−15× enhancement was predicted, depending on how energy transfer changed in the presence of a plasmon. A similar study on an aluminum ring nanocavity calculated a 34× enhancement of upconversion emission at 360 nm from $NaYF_4/Yb^{3+}$, Tm^{3+}.[45] Note that four photons are required to populate this particular transition, and it is therefore more susceptible to incident field enhancement than two-photon upconversion. While theoretical investigations of plasmon-enhanced upconversion have mainly attempted to predict the properties of a specific plasmonic geometry, modeling can also be used to design plasmonic structures to optimize upconversion enhancements.[46] Recent development of more realistic rate equation models for lanthanide upconversion[47] may facilitate better understanding and more accurate prediction of the effect of a plasmon near that class of upconverting material. Extending studies of isolated plasmonic structures to multiparticle simulations[48] may allow consideration of the effects of coupling and multiparticle scattering on upconversion emission.

While many properties of plasmon-enhanced upconversion are system-specific, two processes are general to all upconverting materials: absorption and emission. We next

dx.doi.org/10.1021/jz5019042 | J. Phys. Chem. Lett. 2014, 5, 4020−4031

introduce how plasmons with resonances matched to upconverter absorption and emission may alter the upconversion efficiency.

Plasmon Resonances Matched to Absorption. Formally, the transition rate γ from state $|i\rangle$ to state $|f\rangle$ can be described with Fermi's golden rule[27]

$$\gamma_{if} = \frac{2\pi}{\hbar} |\langle f|\mathbf{E}\cdot\mathbf{p}|i\rangle|^2 \rho_f \quad (1)$$

where $\hbar$ is the reduced Planck's constant, $\mathbf{E}$ is the local electric field, $\mathbf{p}$ is the transition dipole moment, and ρ_f is the density of final states. By increasing $\mathbf{E}$, a plasmon is expected to increase the transition rate to the final state and subsequently increase emission intensity. In general, the emitted light intensity I is proportional to $\mathbf{E}^{2n}$ for an n-photon process. The greater the number of photons necessary to populate the emitting state, the more sensitive the emission intensity will be to any change in $\mathbf{E}$.

Figure 2 illustrates field intensity enhancements and modified rates resulting from a single core−spacer−shell upconverter/plasmon nanoparticle, as calculated using boundary element method (BEM) simulations.[49,50] This nanoparticle is composed of a 70 nm $NaYF_4$ upconverting nanoparticle (n = 1.48), a 15 nm silica spacer layer (n = 1.54), and a 3 nm gold shell (Figure 2a). As seen in Figure 2b, the primary resonance of the particle is at 976 nm, matched to the peak of Yb^{3+} absorption. The absorption and scattering cross sections, normalized to the antenna's geometric area, indicate that the particle absorbs and scatters light with an effective cross section larger than its physical size. Accordingly, the nanoparticle can serve as a nanoantenna at its resonant wavelength.

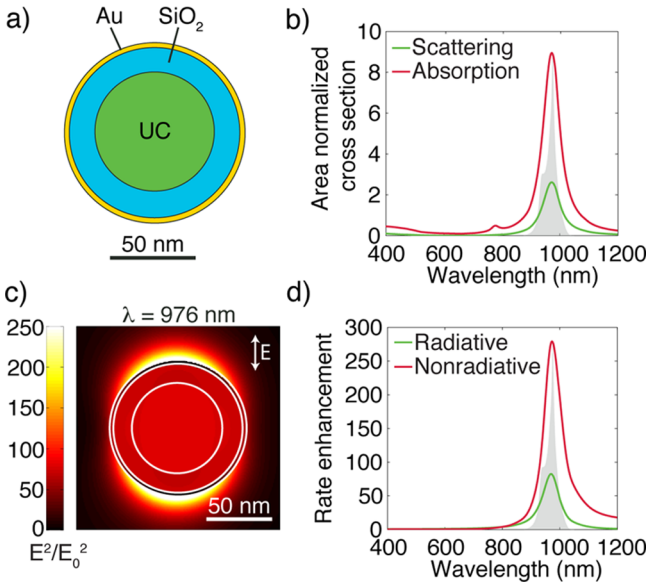

Figure 2. BEM simulations of a single core−shell nanoantenna. (a) Illustration of a structure modeled: 70 nm $NaYF_4$ upconverting nanoparticle (n = 1.48) with a 15 nm silica spacer layer (n = 1.54) and a 3 nm gold shell. (b) Area-normalized scattering and absorption cross sections with Yb^{3+} absorption overlaid in gray. (c) Electric field intensity enhancement at 976 nm. (d) Decay rate enhancements calculated for a dipole emitter located at the center of the core, normalized to emission rates in vacuum, with Yb^{3+} absorption overlaid.

Figure 2c shows the electric field intensity enhancement at 976 nm. The incident field is concentrated both near and in the antenna, with an intensity enhancement of 80× inside of the core (at the position of the upconverter). If no other factors were at play, we would expect the field enhancement to result in a 6400× enhancement in emission intensity at low excitation powers. As discussed above, however, complexity arises from the fact that upconversion proceeds through multiple intermediate states to populate the final emitting state. Each of these transitions has competing decay pathways, which may in turn be influenced by a metallic nanostructure.

To quantify this competing effect at the absorption wavelength, in Figure 2d, we have plotted the change in decay rate experienced by a dipole emitter located at the center of the core. Both radiative and nonradiative decay rates are enhanced, leading to a greater than 300× increase in total decay rate at 976 nm. This rate enhancement is expected to lead to faster depopulation of the intermediate excited states, decreasing the upconversion efficiency and competing with the field intensity enhancement.

Plasmon Resonances Matched to Emission. We next examine the effect of a plasmon resonance matched to the upconverter emission wavelength. Consider an emitter with quantum yield $\eta = \gamma_{rad}/(\gamma_{rad} + \gamma_{nonrad})$, where γ_{rad} and γ_{nonrad} are the radiative and nonradiative decay rates of the transition, respectively. Note that the emitter quantum yield is related but not equivalent to the upconversion efficiency. The former accounts only for decay rates from the final emitting state, while the latter incorporates the efficiency of all processes after absorption (e.g., energy transfer). The emitter quantum yield has a maximum value of 1, while, as noted before, the upconversion efficiency has a maximum value of 0.5 for two-photon upconversion.

The light intensity I emitted by a transition with frequency ω is $I = \hbar\omega\gamma_{rad}$. As γ_{rad} increases, so too does the intensity emitted. In terms of emitter quantum yield, $I = \hbar\omega\eta(\gamma_{rad} + \gamma_{nonrad})$. A plasmonic structure can contribute to both the radiative and nonradiative decay rates. The emitter quantum yield in the presence of a plasmon resonance becomes

$$\eta' = \frac{\gamma'_{rad}}{\gamma'_{rad} + \gamma'_{nonrad}} \quad (2)$$

where prime denotes a plasmon-modified quantity. Each of these plasmon-influenced rates may be decomposed into parts that originate from different constituent mechanisms. The plasmon-influenced radiative decay rate is $\gamma'_{rad} = \gamma^0_{rad} + \gamma^P_{rad}$, where γ^0_{rad} is the intrinsic radiative decay rate and γ^P_{rad} the contribution from the plasmon resonance. Likewise, with the nonradiative decay rate, $\gamma'_{nonrad} = \gamma^0_{nonrad} + \gamma^P_{nonrad}$, we can write

$$\eta' = \frac{\gamma^0_{rad} + \gamma^P_{rad}}{\gamma^0_{rad} + \gamma^0_{nonrad} + \gamma^P_{rad} + \gamma^P_{nonrad}} \quad (3)$$

We define the radiative rate enhancement as $F_{rad} = \gamma^P_{rad}/\gamma^0_{rad}$. Likewise, the nonradiative rate enhancement is $F_{nonrad} = \gamma^P_{nonrad}/\gamma^0_{nonrad}$, which accounts for any quenching by the metallic nanostructure. Substituting $\gamma^P_{rad} = \gamma^0_{rad}F_{rad}$ and $\gamma^P_{nonrad} = \gamma^0_{nonrad}F_{nonrad}$ into eq 3, we can express the emitter quantum yield in the presence of a plasmon η' in terms of the intrinsic emitter quantum yield $\eta^0 = \gamma^0_{rad}/(\gamma^0_{rad} + \gamma^0_{nonrad})$ and the rate enhancements

$$\eta' = \frac{\eta_0(1 + F_{rad})}{1 + F_{nonrad} + \eta_0(F_{rad} - F_{nonrad})} \quad (4)$$

dx.doi.org/10.1021/jz5019042 | J. Phys. Chem. Lett. 2014, 5, 4020−4031

Equation 4 gives two important insights to plasmon-enhanced emission. As a visual aid, we have plotted the results of eq 4 in Figure 3, with F_{rad} set to 10. First, the balance

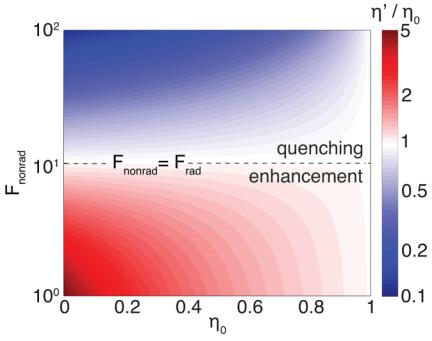

Figure 3. Colormap showing the ratio of the plasmon-modified emitter quantum yield to the intrinsic emitter quantum yield (η'/η_0) versus the intrinsic quantum yield η_0 and nonradiative decay rate enhancement F_{nonrad}. The radiative decay rate enhancement F_{rad} is set to 10, and the dotted line indicates where $F_{rad} = F_{nonrad}$. The color bar is a log scale.

between the radiative rate enhancement and the nonradiative rate enhancement is crucial in determining if there will be a net increase in the quantum yield. If $F_{nonrad} > F_{rad}$, the plasmon contribution to decay rates will result in a net decrease in the quantum yield. This effect can be seen in the upper half of Figure 3, where $F_{nonrad} > F_{rad}$.

The second insight from eq 4, as seen in Figure 3, is that the intrinsic emitter quantum yield η_0 weighs heavily in the possible quantum yield enhancement. If the starting upconverting material has an intrinsic emitter quantum yield approaching 1, there is less room for improvement even when the radiative rate enhancement is large compared to the nonradiative rate enhancement. Conversely, for low emitter quantum yield upconverters, such as lanthanide ions, potential enhancements are greater.

In summary, plasmon-enhanced upconversion requires consideration of important factors besides simply enhanced incident fields and enhanced radiative decay. These factors include modified decay from intermediate states, power dependence, radiative versus nonradiative rate enhancements, and intrinsic emitter quantum yield. Now that we have discussed the theoretical basis for plasmon-enhanced upconversion, we next turn our attention to the state of the art in experimental investigations.

Experimental Investigations. To date, many plasmonic geometries have been employed to modify upconversion emission. It is challenging to directly compare different approaches due to the variability in experimental parameters chosen and reported. For example, one key parameter is the incident power density. Due to the change in power dependence of upconversion at increasing power densities, absorption-matched plasmons are expected to be more effective in enhancing upconversion at lower power densities. As an example, a recent study illustrates this effect. Upconverting nanoparticles were dispersed over absorption-matched silver gratings. At power densities below 2 kW/cm^2, a 38.8× enhancement of upconverted red emission was observed, while at power densities above 40 kW/cm^2, the enhancement fell to 4.4×.[51] Clearly, the excitation power density can dramatically change the enhancement observed. Additionally, understanding the power dependence of plasmonic enhancement can allow better interpretation of its mechanism. Unfortunately, most measurements of plasmon-influenced upconversion to date are reported at just one input power, and often, the power density of the measurement is not reported. Another key parameter to consider when assessing plasmon-enhanced upconversion is the intrinsic upconversion efficiency of the material studied. Lower-efficiency materials have more to gain from plasmons and therefore may present larger enhancements.

Taking these important caveats into account, Figure 4 highlights key examples of different geometries explored and

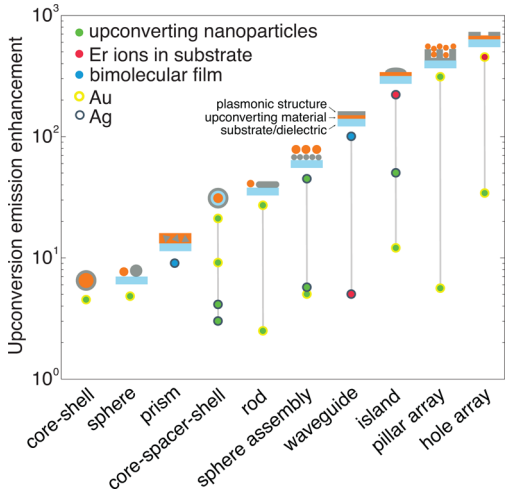

Figure 4. Enhancements reported for two-photon upconversion from lanthanide-doped upconverting nanoparticles (green dots), erbium-doped substrates (red dots), and bimolecular films (blue dots) using a variety of plasmonic geometries. The plasmonic material is indicated with either a yellow (gold) or gray (silver) ring. Schematics of each geometry's cross section are included, with gray indicating a plasmonic material, orange indicating an upconverting material, and blue indicating a substrate or dielectric spacer. References for each column (from top to bottom if more than one reference): core−shell,[52] sphere,[53] prism,[54] core−spacer−shell,[55,56] rod,[57] sphere assembly,[58,59] waveguide,[60,61] island,[62−64] pillar array,[65,66] hole array.[67,68]

enhancements achieved for two-photon upconversion from various materials. The power density and intrinsic upconversion efficiency are not reported frequently enough to allow us to normalize the enhancements observed to these key parameters. We define upconversion enhancement as the integrated intensity of upconversion emission in the presence of a plasmonic material normalized to the integrated emission intensity in the absence thereof. While Figure 4 serves best as a visual summary of experimental reports rather than a quantitative comparison between studies, we can nonetheless gain some important insight about different plasmonic materials and geometries.

Among plasmonic geometries considered to date, most can be categorized as either localized resonators (spheres, core−shell particles, prisms, and rods) or extended structures (sphere assemblies, waveguides, and arrays). The relative arrangement of the upconverter and nanoantenna varies considerably, including upconverter-encapsulated nanoantennas, nanoantenna-encapsulated upconverters, vertically stacked layers of the two materials, and coplanar arrangements of upconverters and nanoantennas. The geometric arrangement and illumination

dx.doi.org/10.1021/jz5019042 | J. Phys. Chem. Lett. 2014, 5, 4020−4031

conditions dictate both the plasmonic modes that can be excited as well as the degree of interaction between the nanoantenna and emitter. The fraction of emitter volume in the position of maximum enhancement will also change the measured enhancements. A large volume of upconverters far from the plasmonic structure (e.g., in a thick film of upconverting material) may diminish the enhancement observed. Judicious sample preparation is important to achieve optimal plasmonic enhancement for a given set of experimental conditions.

Figure 4 shows that silver and gold are the most extensively studied plasmonic materials for upconversion enhancement. Of the two, neither shows a clear advantage. Silver has a stronger plasmonic response than gold because its plasmon resonance is not damped by overlapping interband transitions.[69] Nevertheless, using silver does not consistently result in greater enhancement of upconversion emission, suggesting that other factors such as spectral overlap or field overlap have a greater effect on the enhancements observed. In the future, use of alternative plasmonic materials such as semimetals[70] and highly doped semiconductors[71,72] may also lead to enhanced upconversion.

The maximum enhancement of 450× shown in Figure 4 is observed for a gold hole array patterned over Er^{3+}-doped sapphire.[67] In such a geometry, plasmons at the gold/sapphire interface can be localized in the optical cavity formed by the hole, leading to high near-field enhancements on resonance. When this resonance is matched to the laser pump wavelength at 1480 nm, upconverted emission from Er^{3+} at 980 nm is enhanced. Another high enhancement of upconversion emission was observed on a disk/pillar array. By confining the upconverting emitters to gap regions of high intensity near resonant gold disks, strong near-field enhancement of excitation light was achieved, leading to upconversion enhancements of up to 310×.[65]

In general, control over emitter position is crucial to observe maximum upconversion enhancement as the field enhancement, excitation rate enhancement, and quenching are each highly spatially dependent. For example, studies of the distance dependence of plasmon-modified upconversion emission have found a narrow window for optimal enhancement. In one case, researchers controlled the separation between upconverting nanoparticles and films of 5 nm metal nanospheres using an atomic layer deposited dielectric layer. Maximum upconversion enhancement of 45× occurred at a separation distance of 10 nm for silver spheres.[58] By either decreasing or increasing the separation by 5 nm, the enhancement observed dropped below 5×. Similar studies of silver islands[73] and core−spacer−shell particles[74] also showed a strong dependence on spacing distance. Some of the more modest enhancements in Figure 4 may be the result of unoptimized experimental geometries.

Microscopy-correlated single-particle measurements can further elucidate the importance of emitter positioning. Particularly in anisotropic systems, the relative position and polarization can influence antenna−emitter interaction. In a study of a single upconverting nanoparticle near a single gold nanosphere, the observed enhancement was found to range between 2 and 4.8× depending on the arrangement of the two particles with respect to the incident polarization.[53] More recently, single heterodimers composed of upconverting nanoparticles positioned at the tips of gold nanorods were studied under two illumination polarizations, first along the length of the rod, exciting a mode resonant with upconverter absorption, and then 90° offset. The polarization along the length yielded up to 6× more intense upconversion emission than the perpendicular polarization in the power range studied.[75] Such findings underscore the importance of controlling the three-dimensional architecture of nanoantenna−upconverter systems.

Most studies to date have used lanthanide systems as the upconverting material rather than bimolecular upconverters. Bimolecular upconverters were initially developed in solution, allowing for efficient intermolecular energy transfer but limiting the possibilities for controlled plasmon−emitter interactions. Advances in the synthesis of novel bimolecular upconverting films[9] may enable many more studies of the interaction of these materials with plasmonic structures beyond the few that have been performed to date.[54,60] Note also that many of the emitter molecules chosen for bimolecular upconversion have high emission quantum yield (e.g., for DPA, η = 0.95[76]) and consequently have less to benefit from emission-matched plasmonic enhancements than do the lanthanide ions.

We next explore the role of spectral overlap between the plasmon resonance and emitter. Luminescence enhancement depends on the degree of spectral overlap of the plasmon resonance with emission and absorption. In Figure 5, we have

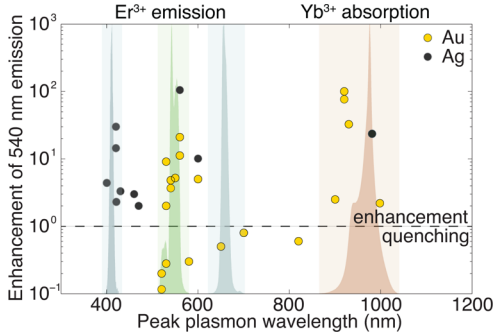

Figure 5. Plasmon wavelength dependence of Er^{3+} upconversion enhancement at 540 nm with Yb^{3+} absorption and Er^{3+} emission peaks overlaid. References are listed in Table 1.

plotted upconversion enhancements versus the plasmon resonance wavelength. For simplicity, we have chosen to focus only on studies of the enhancement of Er^{3+} emission at 540 nm upon excitation at 980 nm. The Yb^{3+} absorption and Er^{3+} emission peaks are overlaid on the plot to show spectral overlap. For clarity, each emission peak is normalized, but we note that the Er^{3+} emission peak at 400 nm is a multiple photon emission peak much weaker than those at 540 and 660 nm. Note that though some structures included exhibit multiple or broad-band resonances, we chose to plot only the peak of the primary plasmon resonance reported. In the next section, we discuss both the absorption-matched and emission-matched cases.

Absorption-Matched Resonances. The three types of structures fabricated to date that exhibit resonances matching Yb^{3+} absorption are pillar arrays, hole arrays, and core−shell particles. For the particular upconversion transition under examination in Figure 5 (980 to 540 nm), a hole array with a plasmon resonance at 930 nm enhanced emission by 30×.[68] Full-field simulations showed that the main contribution to this enhanced emission was a 36× enhancement in field intensity at the center of the hole. This intensity enhancement was tempered by a simultaneous enhancement of the total decay

dx.doi.org/10.1021/jz5019042 | J. Phys. Chem. Lett. 2014, 5, 4020−4031

Table 1. Data from Figure 5

plasmon resonance (nm)	emission enh. at 540 nm	upconverting material	shape[a]	plasmonic material	ref
400	4.4	β-$NaYF_4$/Yb, Er, 28 nm	CSS	Ag	56
420	2.3	β-$NaYF_4$/Yb, Er, 30 nm	nanowires	Ag	101
420	30	β-$NaYF_4$/Yb, Er, 30 nm	SA	Ag	58
420	14.4	β-$NaYF_4$/Yb, Er, 45 nm	CSS	Ag	74
430	3.3	β-$NaYF_4$/Gd, Yb, Er, ~75 × 400 nm	islands	Ag	73
460	3	β-$NaYF_4$/Yb, Er, 90 nm	CSS	Ag	55
470	2	Er-doped $PbO-GeO_2$	spheres	Ag	102
520	0.2	β-$NaYF_4$/Yb, Er, 20 nm	CSS	Au	103
530	9.1	β-$NaYF_4$/Yb, Er, 28 nm	CSS	Au	56
530	2	α-$NaYF_4$/Yb, Er	CS	Au	83
530	0.28	β-$NaGdF_4$/Yb, Er	CSS	Au	80
540	4.8	$NaYF_4$/Yb, Er, 30 nm	sphere	Au	53
550	5.2	β-$NaYF_4$/Yb, Er, 30 nm	SA	Au	58
560	105	Er-doped Al_2O_3	islands	Ag	62
560	21	β-$NaYF_4$/Yb, Er, 90 nm	CSS	Au	55
560	11.2	β-$NaYF_4$/Yb, Er, 90 nm	rod	Au	57
580	0.3	β-$NaYF_4$/Yb, Er, 30 nm	CSS	Au	77
600	10.1	Er-doped bismuth germanate	sphere	Ag	104
600	5	β-$NaYF_4$/Yb, Er, ~250 nm	islands	Au	64
700	0.8	β-$NaYF_4$/Yb, Er, 140 nm	CSS	Au	46
650	0.5	β-$NaYF_4$/Yb, Er, 30 nm	CSS	Au	77
700	0.8	β-$NaYF_4$/Yb, Er, 140 nm	CSS	Au	46
820	0.6	β-$NaYF_4$/Yb, Er, 30 nm	CSS	Au	77
900	2.5	β-$NaYF_4$/Yb, Er, 30 nm	CSS	Au	77
920	100	β-$NaYF_4$/Yb, Er, 25 nm	pillars	Au	65
930	32.6	β-$NaYF_4$/Yb, Er, ~70 nm	holes	Au	68
980	25	β-$NaYF_4$/Yb, Er, 32 nm	grating	Ag	51
998	2.2	β-$NaYF_4$/Yb, Er, 65 nm	pillars	Au	105

[a]CSS = core−spacer−shell, SA = sphere assembly, CS = core−shell.

rate of the intermediate state (similar to the effect discussed alongside Figure 2), leading to an overall excitation enhancement of 35×. The core−shell structure showed a broad absorption peaking at 900 nm and yielded a modest upconversion enhancement of 3×.[77] This enhancement is much less than expected based purely on the field enhancement (our own full-field simulations predict 36×) but also more than expected given the dramatically enhanced decay rates at 980 nm (where our full-field simulations predict 100× enhanced decay rates). These discrepancies highlight the difficulty of accurately predicting the effect of plasmonic structures on upconversion emission using existing techniques. Finally, a gold pillar array evaporated over dielectric posts supported a mode at 920 nm and resulted in a ~100× increase in Er^{3+} emission at 540 nm.[65] Interestingly, pillar arrays with resonances better matched to excitation at 980 nm showed weaker enhancement than the array resonant at 920 nm. Further theoretical and experimental study of the balance between absorption matching for field enhancement and absorption matching leading to fast depopulation of intermediate states may explain these observations.

Even if the peak of the plasmon resonance is not matched to absorption, an incident field enhancement is often invoked to explain observed emission modifications. Measurements of the rise time to populate emitting states can be performed, with a shortening of rise time typically interpreted as evidence for stronger excitation fields.[53,58] The time necessary to populate the emitting state in upconversion depends on the mechanism as well as excitation intensity, however, and changing the latter can also change the former. This complication may lead to a nonintuitive increase in rise time with increasing field enhancements.[78,79] Pump power dependence of the emission intensity can clarify the upconversion mechanism.[40] A useful approximation for field enhancement can be made by comparing the pump power necessary for upconversion emission with a particular intensity I_0 in the control versus the plasmon-enhanced sample.[67] This approximation breaks down, however, if the plasmonic structure has modes overlapping with emission that may be influencing decay rates.

Emission-Matched Resonances. Structures with resonances overlapping with the green emission band in Figure 5 illustrate the delicate balance between enhancement and quenching in this region. For example, a 22× increase in green emission was observed for a core−spacer−shell architecture resonant at 530 nm.[55] A similar geometry with a peak resonance red-shifted to 580 nm quenched upconverted emission.[77] Our own full-field simulations of a 530 nm resonant particle predicted no change in incident field and a 5× enhancement in radiative decay. These simulations underestimate the enhancement observed experimentally, highlighting the need for more comprehensive modeling of plasmon-enhanced upconversion (e.g., calculating rate changes at all positions throughout the core rather than just the center) or for taking nonoptical effects into account (e.g., surface-passivating effects of the dielectric spacer material).

To probe the effect of emission-matched plasmonic nanostructures on decay rates, time-resolved emission measurements are particularly useful. The total decay rate is the sum of the radiative and nonradiative decay rates, and a change to the measured (i.e., total) lifetime can indicate a change to either or

dx.doi.org/10.1021/jz5019042 | J. Phys. Chem. Lett. 2014, 5, 4020−4031

both of its components. For example, a lifetime decrease from 300 to 200 μs in emission at 540 nm was measured for core−spacer−shell particles.[80] This decrease coincided with emission quenching and was therefore attributed to enhanced nonradiative decay. On the other hand, a decrease in decay lifetime coincident with an increase in emission suggests radiative rate enhancements. This type of shortening was observed for silver nanoparticles attached to the surface of upconverting nanoparticles.[56]

To our knowledge, the largest measured change in decay lifetime for plasmon-modified lanthanide upconversion is 8×.[51,65] For low quantum yield transitions such as visible upconversion emission from Er^{3+}, the intrinsic nonradiative decay rate is much faster than the radiative decay rate.[58] The change in nonradiative decay lifetime may therefore dominate the change in total decay lifetime. An experimental challenge is to deconvolute changes to the radiative and nonradiative decay pathways to quantitatively assess the influence of plasmons on upconversion quantum yield. A second challenge is to enhance the radiative rate without changing the nonradiative rate. One possible strategy is using more intricate plasmonic geometries such as nanocrescents, which promise emission-matched radiative rate enhancements of over 100×.[81]

The highest enhancement in the emission-matched region of Figure 5 was ∼100×, observed for silver islands patterned over an Er^{3+}-doped alumina substrate.[62] Though the maximum absorption for this structure was at 520 nm, the islands showed broad absorption out to the near-infrared. Different island films with similar absorption in the visible and less absorption in the infrared showed diminished enhancements, leading the authors to conclude that incident field intensity enhancements contributed to the overall increase in emission.

Absorption- and Emission-Matched Resonances. Structures that promise simultaneous enhancement of absorption and emission are particularly ripe for further exploration. A recent example of this approach is a gold pillar array designed with modes at both 980 and 700 nm (overlapping with Tm^{3+} emission), leading to a 4× enhancement of upconversion emission.[66] The introduction of emission-matched modes risks quenching of upconverted light, however, and it will be useful to differentiate between the absorption and emission modifications in such structures. A creative way to do so experimentally is to compare upconversion and photoluminescence measurements.[62] Exciting at a higher energy to study photoluminescence can isolate the influence of modified decay rates independently of absorption enhancements. Alternatively, exciting at one wavelength and measuring both upconversion and photoluminescence (e.g., exciting Er^{3+} at 980 nm and measuring emission at 1550 and 540 nm) can also offer insight into the relative contributions of absorption and emission effects.

Nonoptical Effects. We briefly discuss nonoptical side effects of metal nanostructures that may influence or even dominate the observed change in emission with the addition of a plasmonic structure.

Solution-Phase Measurements. Challenges particular to measurements performed in solution rather than on a substrate include scattering and Brownian diffusion of emitters in and out of the regions of high field intensity.[82] The latter results in an averaging out of plasmonic effects. Furthermore, in solution, direct contact between the emitters and metal nanoparticles can lead to quenching. These issues would dampen the observable enhancement and may explain why plasmon-enhanced bimolecular upconversion in solution has not been reported. Diffusion can be avoided in the case of upconverting nanoparticles measured in solution, where the position of the emitter can be fixed relative to the nanoantenna using dielectric spacer layers.[55,57] These measurements may still suffer from decreased collection efficiency due to scattering in solution.

Chemical Effects. As mentioned earlier, a gold shell grown around an upconverting nanoparticle was shown to enhance the emission intensity while increasing the emission lifetime.[56] This unexpected result was attributed to reduced surface recombination from the growth of a passivating metal shell. Metal nanostructures may also change the electronic properties of the upconverting emitter, for example, by locally modifying the crystal field of the host lattice.[83]

Heating. Illuminating a plasmonic structure can result in strong local heating, particularly on resonance.[84] Meanwhile, lanthanide upconversion is temperature-dependent in certain temperature ranges.[85−87] This temperature dependence has two origins. First, in solid-state host lattices, the number of phonons increases with temperature, increasing the probability of nonradiative relaxation. As a result, decay lifetimes and pathways change with temperature. Second, certain emitting states can be thermally populated. For example, the green-emitting $^4S_{3/2}$ and $^4H_{11/2}$ states in Er^{3+} are closely spaced in energy, and the ratio of their respective emission intensities increases predictably according to a Boltzmann distribution. In fact, it is possible to track the temperature change in a plasmon-heated upconverting sample by monitoring the intensity ratio of these two emission peaks.[59] This effect can be manipulated for integrated heating/temperature sensing with ∼1 K resolution in between 300 and 1050 K.[88]

Bimolecular upconversion in polymer films is also strongly temperature-dependent.[89] Through local heating, a plasmonic nanostructure can increase diffusion and enable more efficient energy transfers, leading to upconversion. Conversely, at higher temperatures, changes in polymer morphology or decomposition of active dyes can decrease the emission intensity. Furthermore, increasing temperature can decrease the lifetime of intermediate states, decreasing the emission intensity as well.[60,90] If plasmonic heating in nanoantenna−upconverter composites can be better understood, it could be used not only to maximize upconversion enhancements but also in applications such as photothermal therapy and imaging.[91,92]

In the past 5 years, research in plasmon-enhanced upconversion has gained great momentum, with a plethora of upconverter−plasmon geometries showing enhanced emission.

Outlook. In the past 5 years, research in plasmon-enhanced upconversion has gained great momentum, with a plethora of upconverter−plasmon geometries showing enhanced emission. Experimental and theoretical studies of the factors influencing plasmon-modified upconversion, particularly regarding field overlap and spectral overlap, have started to clarify design principles for optimal plasmon−emitter interaction. Many opportunities for exploration remain, and we conclude with two questions that we find especially important and interesting for further study. First, how do plasmonic structures influence energy transfer in upconversion? Studies of various Förster

dx.doi.org/10.1021/jz5019042 | J. Phys. Chem. Lett. 2014, 5, 4020−4031

energy-transfer processes (e.g., with dyes,[93−95] quantum dots,[96] and ions[97,98]) have shown that by modifying transition rates, nanophotonic engineering can change the efficiency of energy transfer. Longer-range (>1 nm) energy transfer is more highly influenced by a changed nanophotonic environment than short-range transfers.[99] For $NaYF_4$/18% Yb^{3+}, 2% Er^{3+}, it has been proposed that energy transfer to Er^{3+} acceptors in an intermediate excited state has a transfer radius of 3.4 nm and could therefore be influenced by a plasmon resonance.[51] Further examination of plasmon-enhanced upconversion at different doping densities may elucidate this effect and help improve modeling of the process. Second, what upconversion efficiencies are necessary for applications? In the recent literature, two of the most popular applications for upconverting materials are sub-band-gap absorption in photovoltaics and new bioimaging probes. Quantitative modeling exploring the magnitude of efficiency enhancement necessary to meaningfully increase solar cell efficiency can serve as both a reality check and a roadmap for efficiency targets.[100] Similar work for specific bioimaging and therapeutic applications could prove highly useful in guiding the development of upconverting materials.

In 2004, Auzel concluded his comprehensive review of upconversion stating, "If there was some general philosophy to derive from this review, it would be that upconversion is an endless field." Ten years later, plasmon-enhanced upconversion is just one of many innovative approaches to improving upconverters, and the field still seems endless indeed. While the principle of plasmon-enhanced upconversion has been well-established, there remain many exciting topics of study in the design of plasmon−upconverter composites.

AUTHOR INFORMATION

Corresponding Author

*E-mail: jdionne@stanford.edu.

Notes

The authors declare no competing financial interest.

Biographies

Di Meng Wu is a Ph.D. candidate in the Department of Chemistry at Stanford University working in the Salleo and Dionne research groups. She received her B.A. in Chemistry from Cornell University in 2009. She studies optical and chemical approaches to enhancing upconversion emission.

Aitzol García-Etxarri is a postdoctoral researcher in the Dionne research group at Stanford University. He received his Ph.D. in Physics from the University of the Basque Country in 2010. He researches novel applications of optical antennas for enhanced nanoscale control of electromagnetic fields.

Alberto Salleo is an associate professor of Materials Science and Engineering at Stanford University. His research group (http://salleo.stanford.edu) studies novel materials for large-area and flexible electronic/photonic devices and structure/property relations of polymeric semiconductors and nanostructured materials. He is the recipient of the NSF CAREER Award, the 3M Untenured Faculty Award, and the SPIE Early Career Award.

Jennifer Dionne is an assistant professor of Materials Science and Engineering at Stanford University. Her research team (http://dionne.stanford.edu) develops new optical materials and tools to visualize and control nanoscale systems and phenomena, particularly those relevant to renewable energy and biology. This work has been recognized with the Presidential Early Career Award and the Kavli Nanoscience Lectureship.

ACKNOWLEDGMENTS

The authors thank Gururaj Naik and all members of the Dionne group for helpful feedback on the manuscript. This work is supported by a U.S. Department of Energy SunShot award (DE-EE0005331) and the Global Climate and Energy Project. Support from Stanford's TomKat Center for Sustainable Energy is also gratefully acknowledged. D.M.W. acknowledges support from the National Science Foundation Graduate Research Fellowship Program and the Gabilan Stanford Graduate Fellowship.

REFERENCES

(1) Gargas, D. J.; Chan, E. M.; Ostrowski, A. D.; Aloni, S.; Altoe, M. V. P.; Barnard, E. S.; Sanii, B.; Urban, J. J.; Milliron, D. J.; Cohen, B. E.; et al. Engineering Bright Sub-10-nm Upconverting Nanocrystals for Single-Molecule Imaging. *Nat. Nanotechnol.* **2014**, *9*, 300−305.

(2) Chen, G.; Qiu, H.; Prasad, P. N.; Chen, X. Upconversion Nanoparticles: Design, Nanochemistry, and Applications in Theranostics. *Chem. Rev.* **2014**, *114*, 5161−5214.

(3) Wang, L.; Dong, H.; Li, Y.; Xue, C.; Sun, L.-D.; Yan, C.-H.; Li, Q. Reversible Near-Infrared Light Directed Reflection in a Self-Organized Helical Superstructure Loaded with Upconversion Nanoparticles. *J. Am. Chem. Soc.* **2014**, *136*, 4480−4483.

(4) Jiang, Z.; Xu, M.; Li, F.; Yu, Y. Red-Light-Controllable Liquid-Crystal Soft Actuators via Low-Power Excited Upconversion Based on Triplet−Triplet Annihilation. *J. Am. Chem. Soc.* **2013**, *135*, 16446−16453.

(5) Huang, X.; Han, S.; Huang, W.; Liu, X. Enhancing Solar Cell Efficiency: The Search For Luminescent Materials as Spectral Converters. *Chem. Soc. Rev.* **2012**, *42*, 173.

(6) Gray, V.; Dzebo, D.; Abrahamsson, M.; Albinsson, B.; Moth-Poulsen, K. Triplet−Triplet Annihilation Photon-Upconversion: Towards Solar Energy Applications. *Phys. Chem. Chem. Phys.* **2014**, *16*, 10345.

(7) Zhao, J.; Jin, D.; Schartner, E. P.; Lu, Y.; Liu, Y.; Zvyagin, A. V.; Zhang, L.; Dawes, J. M.; Xi, P.; Piper, J. A.; et al. Single-Nanocrystal Sensitivity Achieved by Enhanced Upconversion Luminescence. *Nat. Nanotechnol.* **2013**, *8*, 729−734.

(8) Li, X.; Zhang, F.; Zhao, D. Highly Efficient Lanthanide Upconverting Nanomaterials: Progresses and Challenges. *Nano Today* **2013**, *8*, 643−676.

(9) Simon, Y. C.; Weder, C. Low-Power Photon Upconversion through Triplet−Triplet Annihilation in Polymers. *J. Mater. Chem.* **2012**, *22*, 20817.

(10) Zhao, J.; Ji, S.; Guo, H. Triplet−Triplet Annihilation Based Upconversion: From Triplet Sensitizers and Triplet Acceptors to Upconversion Quantum Yields. *RSC Adv.* **2011**, *1*, 937.

(11) Johnson, C. M.; Reece, P. J.; Conibeer, G. J. Slow-Light-Enhanced Upconversion for Photovoltaic Applications in One-Dimensional Photonic Crystals. *Opt. Lett.* **2011**, *36*, 3990−3992.

(12) Herter, B.; Wolf, S.; Fischer, S.; Gutmann, J.; Bläsi, B.; Goldschmidt, J. C. Increased Upconversion Quantum Yield in Photonic Structures Due to Local Field Enhancement and Modification of the Local Density of States — A Simulation-Based Analysis. *Opt. Express* **2013**, *21*, A883.

(13) Zou, W.; Visser, C.; Maduro, J. A.; Pshenichnikov, M. S.; Hummelen, J. C. Broadband Dye-Sensitized Upconversion of Near-Infrared Light. *Nat. Photonics* **2012**, *6*, 560−564.

(14) Pan, A. C.; Del Cañizo, C.; Cánovas, E.; Santos, N. M.; Leitão, J. P.; Luque, A. Enhancement of Up-Conversion Efficiency by Combining Rare Earth-Doped Phosphors with PbS Quantum Dots. *Sol. Energy Mater. Sol. Cells* **2010**, *94*, 1923−1926.

(15) Auzel, F. Upconversion and Anti-Stokes Processes with f and d Ions in Solids. *Chem. Rev.* **2004**, *104*, 139−173.

(16) Page, R.; Schaffers, K.; Waide, P.; Tassano, J.; Payne, S.; Krupke, W.; Bischel, W. Upconversion-Pumped Luminescence Efficiency of

Rare-Earth-Doped Hosts Sensitized with Trivalent Ytterbium. *J. Opt. Soc. Am. B* **1998**, *15*, 996−1008.
(17) Boyer, J.-C.; Van Veggel, F. C. J. M. Absolute Quantum Yield Measurements of Colloidal $NaYF_4$: Er^{3+}, Yb^{3+} Upconverting Nanoparticles. *Nanoscale* **2010**, *2*, 1417−1419.
(18) Wang, F.; Wang, J.; Liu, X. Direct Evidence of a Surface Quenching Effect on Size-Dependent Luminescence of Upconversion Nanoparticles. *Angew. Chem., Int. Ed.* **2010**, *49*, 7456−7460.
(19) Cao, C.; Qin, W.; Zhang, J.; Wang, Y.; Zhu, P.; Wei, G.; Wang, G.; Kim, R.; Wang, L. Ultraviolet Upconversion Emissions of Gd^{3+}. *Opt. Lett.* **2008**, *33*, 857−859.
(20) Wu, S.; Han, G.; Milliron, D. J.; Aloni, S.; Altoe, V.; Talapin, D. V.; Cohen, B. E.; Schuck, P. J. Non-Blinking and Photostable Upconverted Luminescence from Single Lanthanide-Doped Nanocrystals. *Proc. Natl. Acad. Sci. U.S.A.* **2009**, *106*, 10917−10921.
(21) Liu, C.; Hou, Y.; Gao, M. Are Rare-Earth Nanoparticles Suitable for In Vivo Applications? *Adv. Mater.* **2014**, DOI: 10.1002/adma.201305535.
(22) Singh-Rachford, T. N.; Castellano, F. N. Photon Upconversion Based on Sensitized Triplet−Triplet Annihilation. *Coord. Chem. Rev.* **2010**, *254*, 2560−2573.
(23) Khnayzer, R. S.; Blumhoff, J.; Harrington, J. A.; Haefele, A.; Deng, F.; Castellano, F. N. Upconversion-Powered Photoelectrochemistry. *Chem. Commun.* **2012**, *48*, 209.
(24) Smith, K. M.; Falk, J. E. *Porphyrins and Metalloporphyrins*; Elsevier: Amsterdam, The Netherlands, 1975.
(25) Strohhöfer, C.; Polman, A. Absorption and Emission Spectroscopy in Er^{3+}−Yb^{3+} Doped Aluminum Oxide Waveguides. *Opt. Mater.* **2003**, *21*, 705−712.
(26) Raether, H. *Surface Plasmons on Smooth and Rough Surfaces and on Gratings*; Springer: New York, 1988.
(27) Novotny, L.; Hecht, B. *Principles of Nano-Optics*, 2nd ed.; Cambridge University Press: New York, 2012.
(28) Novotny, L.; van Hulst, N. Antennas for Light. *Nat. Photonics* **2011**, *5*, 83−90.
(29) Pelton, M.; Aizpurua, J.; Bryant, G. Metal-Nanoparticle Plasmonics. *Laser Photonics Rev.* **2008**, *2*, 136−159.
(30) García-Etxarri, A.; Apell, P.; Käll, M.; Aizpurua, J. A Combination of Concave/Convex Surfaces for Field-Enhancement Optimization: The Indented Nanocone. *Opt. Express* **2012**, *20*, 25201.
(31) Anger, P.; Bharadwaj, P.; Novotny, L. Enhancement and Quenching of Single-Molecule Fluorescence. *Phys. Rev. Lett.* **2006**, *96*, 113002.
(32) Schuck, P. J.; Fromm, D. P.; Sundaramurthy, A.; Kino, G. S.; Moerner, W. E. Improving the Mismatch between Light and Nanoscale Objects with Gold Bowtie Nanoantennas. *Phys. Rev. Lett.* **2005**, *94*, 017402.
(33) Kneipp, K.; Wang, Y.; Kneipp, H.; Perelman, L. T.; Itzkan, I.; Dasari, R. R.; Feld, M. S. Single Molecule Detection Using Surface-Enhanced Raman Scattering (SERS). *Phys. Rev. Lett.* **1997**, *78*, 1667−1670.
(34) Nie, S.; Emory, S. R. Probing Single Molecules and Single Nanoparticles by Surface-Enhanced Raman Scattering. *Science* **1997**, *275*, 1102−1106.
(35) Neubrech, F.; Pucci, A.; Cornelius, T.; Karim, S.; García-Etxarri, A.; Aizpurua, J. Resonant Plasmonic and Vibrational Coupling in a Tailored Nanoantenna for Infrared Detection. *Phys. Rev. Lett.* **2008**, *101*, 157403.
(36) Haynes, C. L.; Van Duyne, R. P. Plasmon-Sampled Surface-Enhanced Raman Excitation Spectroscopy. *J. Phys. Chem. B* **2003**, *107*, 7426−7433.
(37) Wang, H.; Kundu, J.; Halas, N. J. Plasmonic Nanoshell Arrays Combine Surface-Enhanced Vibrational Spectroscopies on a Single Substrate. *Angew. Chem., Int. Ed.* **2007**, *46*, 9040−9044.
(38) Kinkhabwala, A.; Yu, Z.; Fan, S.; Avlasevich, Y.; Müllen, K.; Moerner, W. E. Large Single-Molecule Fluorescence Enhancements Produced by a Bowtie Nanoantenna. *Nat. Photonics* **2009**, *3*, 654−657.
(39) Pollnau, M.; Gamelin, D. R.; Lüthi, S. R.; Güdel, H. U.; Hehlen, M. P. Power Dependence of Upconversion Luminescence in Lanthanide and Transition-Metal-Ion Systems. *Phys. Rev. B* **2000**, *61*, 3337−3346.
(40) Suyver, J. F.; Aebischer, A.; García-Revilla, S.; Gerner, P.; Güdel, H. U. Anomalous Power Dependence of Sensitized Upconversion Luminescence. *Phys. Rev. B* **2005**, *71*, 125123.
(41) Fischer, S.; Steinkemper, H.; Löper, P.; Hermle, M.; Goldschmidt, J. C. Modeling Upconversion of Erbium Doped Microcrystals Based on Experimentally Determined Einstein Coefficients. *J. Appl. Phys.* **2012**, *111*, 013109.
(42) Esteban, R.; Laroche, M.; Greffet, J.-J. Influence of Metallic Nanoparticles on Upconversion Processes. *J. Appl. Phys.* **2009**, *105*, 033107.
(43) Fischer, S.; Hallermann, F.; Eichelkraut, T.; von Plessen, G.; Krämer, K. W.; Biner, D.; Steinkemper, H.; Hermle, M.; Goldschmidt, J. C. Plasmon Enhanced Upconversion Luminescence near Gold Nanoparticles — Simulation and Analysis of the Interactions. *Opt. Express* **2012**, *20*, 271−282.
(44) Fischer, S.; Hallermann, F.; Eichelkraut, T.; von Plessen, G.; Krämer, K. W.; Biner, D.; Steinkemper, H.; Hermle, M.; Goldschmidt, J. C. Plasmon Enhanced Upconversion Luminescence Near Gold Nanoparticles — Simulation and Analysis of the Interactions: Errata. *Opt. Express* **2013**, *21*, 10606.
(45) Lantigua, C.; He, S.; Bouzan, M. A.; Hayenga, W.; Johnson, N. J. J.; Almutairi, A.; Khajavikhan, M. Engineering Upconversion Emission Spectra Using Plasmonic Nanocavities. *Opt. Lett.* **2014**, *39*, 3710−3713.
(46) Fujii, M.; Nakano, T.; Imakita, K.; Hayashi, S. Upconversion Luminescence of Er and Yb Codoped $NaYF_4$ Nanoparticles with Metal Shells. *J. Phys. Chem. C* **2013**, *117*, 1113−1120.
(47) Chan, E. M.; Gargas, D. J.; Schuck, P. J.; Milliron, D. J. Concentrating and Recycling Energy in Lanthanide Codopants for Efficient and Spectrally Pure Emission: The Case of $NaYF_4$:Er^{3+}/Tm^{3+} Upconverting Nanocrystals. *J. Phys. Chem. B* **2012**, 10561−10570.
(48) Solís, D. M.; Taboada, J. M.; Obelleiro, F.; Liz-Marzán, L. M.; García de Abajo, F. J. Toward Ultimate Nanoplasmonics Modeling. *ACS Nano* **2014**, *8*, 7559−7570.
(49) García de Abajo, F. J.; Howie, A. Relativistic Electron Energy Loss and Electron-Induced Photon Emission in Inhomogeneous Dielectrics. *Phys. Rev. Lett.* **1998**, *80*, 5180−5183.
(50) García de Abajo, F.; Howie, A. Retarded Field Calculation of Electron Energy Loss in Inhomogeneous Dielectrics. *Phys. Rev. B* **2002**, *65*, 115418.
(51) Lu, D.; Cho, S. K.; Ahn, S.; Brun, L.; Summers, C. J.; Park, W. Plasmon Enhancement Mechanism for the Upconversion Processes in $NaYF_4$:Yb^{3+},Er^{3+} Nanoparticles: Maxwell versus Förster. *ACS Nano* **2014**, *8*, 7780−7792.
(52) Zhang, H.; Li, Y.; Ivanov, I. A.; Qu, Y.; Huang, Y.; Duan, X. Plasmonic Modulation of the Upconversion Fluorescence in $NaYF_4$:Yb/Tm Hexaplate Nanocrystals Using Gold Nanoparticles or Nanoshells. *Angew. Chem., Int. Ed.* **2010**, *49*, 2865−2868.
(53) Schietinger, S.; Aichele, T.; Wang, H.-Q.; Nann, T.; Benson, O. Plasmon-Enhanced Upconversion in Single $NaYF_4$:Yb^{3+}/Er^{3+} Co-doped Nanocrystals. *Nano Lett.* **2010**, *10*, 134−138.
(54) Poorkazem, K.; Hesketh, A. V.; Kelly, T. L. Plasmon-Enhanced Triplet−Triplet Annihilation Using Silver Nanoplates. *J. Phys. Chem. C* **2014**, *118*, 6398−6404.
(55) Kannan, P.; Rahim, F. A.; Teng, X.; Chen, R.; Sun, H.; Huang, L.; Kim, D.-H. Enhanced Emission of $NaYF_4$:Yb,Er/Tm Nanoparticles by Selective Growth of Au and Ag Nanoshells. *RSC Adv.* **2013**, *3*, 7718.
(56) Deng, W.; Sudheendra, L.; Zhao, J.; Fu, J.; Jin, D.; Kennedy, I. M.; Goldys, E. M. Upconversion in $NaYF_4$:Yb, Er Nanoparticles Amplified by Metal Nanostructures. *Nanotechnology* **2011**, *22*, 325604−325604.
(57) Kannan, P.; Rahim, F. A.; Chen, R.; Teng, X.; Huang, L.; Sun, H.; Kim, D.-H. Au Nanorod Decoration on $NaYF_4$:Yb/Tm Nanoparticles for Enhanced Emission and Wavelength-Dependent Biomolecular Sensing. *ACS Appl. Mater. Interfaces* **2013**, *5*, 3508−3513.

(58) Saboktakin, M.; Ye, X.; Oh, S. J.; Hong, S.-H.; Fafarman, A. T.; Chettiar, U. K.; Engheta, N.; Murray, C. B.; Kagan, C. R. Metal Enhanced Upconversion Luminescence Tunable through Metal Nanoparticle−Nanophosphor Separation. *ACS Nano* **2012**, *6*, 8758−8766.
(59) Xu, W.; Xu, S.; Zhu, Y.; Liu, T.; Bai, X.; Dong, B.; Xu, L.; Song, H. Ultra-Broad Plasma Resonance Enhanced Multicolor Emissions in an Assembled Ag/$NaYF_4$:Yb,Er Nano-Film. *Nanoscale* **2012**, *4*, 6971−6973.
(60) Baluschev, S.; Yu, F.; Miteva, T.; Ahl, S.; Yasuda, A.; Nelles, G.; Knoll, W.; Wegner, G. Metal-Enhanced Up-Conversion Fluorescence: Effective Triplet−Triplet Annihilation near Silver Surface. *Nano Lett.* **2005**, *5*, 2482−2484.
(61) Verhagen, E.; Kuipers, L.; Polman, A. Enhanced Nonlinear Optical Effects with a Tapered Plasmonic Waveguide. *Nano Lett.* **2007**, *7*, 334−337.
(62) Aisaka, T.; Fujii, M.; Hayashi, S. Enhancement of Upconversion Luminescence of Er doped Al_2O_3 Films by Ag Island Films. *Appl. Phys. Lett.* **2008**, *92*, 132105.
(63) Xu, W.; Zhu, Y.; Chen, X.; Wang, J.; Tao, L.; Xu, S.; Liu, T.; Song, H. A Novel Strategy for Improving Upconversion Luminescence of $NaYF_4$:Yb, Er Nanocrystals by Coupling with Hybrids of Silver Plasmon Nanostructures and Poly(methyl methacrylate) Photonic Crystals. *Nano Res.* **2013**, *6*, 795−807.
(64) Zhang, H.; Xu, D.; Huang, Y.; Duan, X. Highly Spectral Dependent Enhancement of Upconversion Emission with Sputtered Gold Island Films. *Chem. Commun.* **2010**, *47*, 979.
(65) Zhang, W.; Ding, F.; Chou, S. Y. Large Enhancement of Upconversion Luminescence of $NaYF_4$:Yb^{3+}/Er^{3+} Nanocrystal by 3D Plasmonic Nano-Antennas. *Adv. Mater.* **2012**, *24*, OP236−OP241.
(66) Luu, Q.; Hor, A.; Fisher, J.; Anderson, R. B.; Liu, S.; Luk, T.-S.; Paudel, H. P.; Farrokh Baroughi, M.; May, P. S.; Smith, S. Two-Color Surface Plasmon Polariton Enhanced Upconversion in $NaYF_4$:Yb:Tm Nanoparticles on Au Nanopillar Arrays. *J. Phys. Chem. C* **2014**, *118*, 3251−3257.
(67) Verhagen, E.; Kuipers, L.; Polman, A. Field Enhancement in Metallic Subwavelength Aperture Arrays Probed by Erbium Upconversion Luminescence. *Opt. Express* **2009**, *17*, 14586−14598.
(68) Saboktakin, M.; Ye, X.; Chettiar, U. K.; Engheta, N.; Murray, C. B.; Kagan, C. R. Plasmonic Enhancement of Nanophosphor Upconversion Luminescence in Au Nanohole Arrays. *ACS Nano* **2013**, *7*, 7186−7192.
(69) Amendola, V.; Bakr, O. M.; Stellacci, F. A Study of the Surface Plasmon Resonance of Silver Nanoparticles by the Discrete Dipole Approximation Method: Effect of Shape, Size, Structure, and Assembly. *Plasmonics* **2010**, *5*, 85−97.
(70) Naik, G. V.; Schroeder, J. L.; Ni, X.; Kildishev, A. V.; Sands, T. D.; Boltasseva, A. Titanium Nitride as a Plasmonic Material for Visible and Near-Infrared Wavelengths. *Opt. Mater. Express* **2012**, *2*, 478−489.
(71) Garcia, G.; Buonsanti, R.; Runnerstrom, E. L.; Mendelsberg, R. J.; Llordés, A.; Anders, A.; Richardson, T. J.; Milliron, D. J. Dynamically Modulating the Surface Plasmon Resonance of Doped Semiconductor Nanocrystals. *Nano Lett.* **2011**, *11*, 4415−4420.
(72) Gordon, T. R.; Paik, T.; Klein, D. R.; Naik, G. V.; Caglayan, H.; Boltasseva, A.; Murray, C. B. Shape-Dependent Plasmonic Response and Directed Self-Assembly in a New Semiconductor Building Block, Indium-Doped Cadmium Oxide (ICO). *Nano Lett.* **2013**, *13*, 2857−2863.
(73) Shen, J.; Li, Z. Q.; Chen, Y. R.; Chen, X. H.; Chen, Y. W.; Sun, Z.; Huang, S. M. Influence of SiO_2 Layer Thickness on Plasmon Enhanced Upconversion in Hybrid Ag/SiO_2/$NaYF_4$:Yb, Er, Gd Structures. *Appl. Surf. Sci.* **2013**, *270*, 712−717.
(74) Yuan, P.; Lee, Y. H.; Gnanasammandhan, M. K.; Guan, Z.; Zhang, Y.; Xu, Q.-H. Plasmon Enhanced Upconversion Luminescence of $NaYF_4$:Yb,Er@SiO_2@Ag Core−Shell Nanocomposites for Cell Imaging. *Nanoscale* **2012**, *4*, 5132.
(75) Greybush, N. J.; Saboktakin, M.; Ye, X.; Della Giovampaola, C.; Oh, S. J.; Berry, N. E.; Engheta, N.; Murray, C. B.; Kagan, C. R. Plasmon-Enhanced Upconversion Luminescence in Single Nanophosphor−Nanorod Heterodimers Formed through Template-Assisted Self-Assembly. *ACS Nano* **2014**, *8*, 9482−9491.
(76) Islangulov, R. R.; Kozlov, D. V.; Castellano, F. N. Low Power Upconversion Using MLCT Sensitizers. *Chem. Commun.* **2005**, 3776.
(77) Priyam, A.; Idris, N. M.; Zhang, Y. Gold Nanoshell Coated $NaYF_4$ Nanoparticles for Simultaneously Enhanced Upconversion Fluorescence and Darkfield Imaging. *J. Mater. Chem.* **2011**, *22*, 960.
(78) Liu, N.; Qin, W.; Qin, G.; Jiang, T.; Zhao, D. Highly Plasmon-Enhanced Upconversion Emissions from Au@β-$NaYF_4$:Yb,Tm Hybrid Nanostructures. *Chem. Commun.* **2011**, *47*, 7671−3.
(79) Jiang, T.; Liu, Y.; Liu, S.; Liu, N.; Qin, W. Upconversion Emission Enhancement of Gd^{3+} Ions Induced by Surface Plasmon Field in Au@$NaYF_4$ Nanostructures Codoped with Gd^{3+}−Yb^{3+}−Tm^{3+} Ions. *J. Colloid Interface Sci.* **2012**, *377*, 81−87.
(80) Liu, S.; Chen, G.; Ohulchanskyy, T. Y.; Swihart, M. T.; Prasad, P. N. Facile Synthesis and Potential Bioimaging Applications of Hybrid Upconverting and Plasmonic $NaGdF_4$: Yb^{3+}, Er^{3+}/Silica/Gold Nanoparticles. *Theranostics* **2013**, *3*, 275−281.
(81) Atre, A. C.; García-Etxarri, A.; Alaeian, H.; Dionne, J. A. Toward High-Efficiency Solar Upconversion with Plasmonic Nanostructures. *J. Opt.* **2012**, *14*, 024008.
(82) Ming, T.; Chen, H.; Jiang, R.; Li, Q.; Wang, J. Plasmon-Controlled Fluorescence: Beyond the Intensity Enhancement. *J. Phys. Chem. Lett.* **2012**, *3*, 191−202.
(83) Sudheendra, L.; Ortalan, V.; Dey, S.; Browning, N. D.; Kennedy, I. M. Plasmonic Enhanced Emissions from Cubic $NaYF_4$:Yb: Er/Tm Nanophosphors. *Chem. Mater.* **2011**, *23*, 2987−2993.
(84) Baffou, G.; Quidant, R. Thermo-Plasmonics: Using Metallic Nanostructures as Nano-Sources of Heat. *Laser Photonics Rev.* **2012**, *7*, 171−187.
(85) Suyver, J. F.; Grimm, J.; Krämer, K. W.; Güdel, H. U. Highly Efficient Near-Infrared to Visible Up-Conversion Process in $NaYF_4$:Yb^{3+} Er^{3+}. *J. Lumin.* **2005**, *114*, 53−59.
(86) Wu, K.; Cui, J.; Kong, X.; Wang, Y. Temperature Dependent Upconversion Luminescence of Yb/Er Codoped $NaYF_4$ Nanocrystals. *J. Appl. Phys.* **2011**, *110*, 053510.
(87) Fischer, L. H.; Harms, G. S.; Wolfbeis, O. S. Upconverting Nanoparticles for Nanoscale Thermometry. *Angew. Chem., Int. Ed.* **2011**, *50*, 4546−4551.
(88) Debasu, M. L.; Ananias, D.; Pastoriza-Santos, I.; Liz-Marzán, L. M.; Rocha, J.; Carlos, L. D. All-In-One Optical Heater−Thermometer Nanoplatform Operative from 300 to 2000 K Based on Er^{3+} Emission and Blackbody Radiation. *Adv. Mater.* **2013**, *25*, 4868−4874.
(89) Singh-Rachford, T. N.; Lott, J.; Weder, C.; Castellano, F. N. Influence of Temperature on Low-Power Upconversion in Rubbery Polymer Blends. *J. Am. Chem. Soc.* **2009**, *131*, 12007−12014.
(90) Goudarzi, H.; Keivanidis, P. E. Triplet−Triplet Annihilation-Induced Up-Converted Delayed Luminescence in Solid-State Organic Composites: Monitoring Low-Energy Photon Up-Conversion at Low Temperatures. *J. Phys. Chem. C* **2014**, *118*, 14256−14265.
(91) Dong, B.; Xu, S.; Sun, J.; Bi, S.; Li, D.; Bai, X.; Wang, Y.; Wang, L.; Song, H. Multifunctional $NaYF_4$:Yb^{3+},Er^{3+}@Ag Core/Shell Nanocomposites: Integration of Upconversion Imaging and Photothermal Therapy. *J. Mater. Chem.* **2011**, *21*, 6193.
(92) Idris, N. M.; Gnanasammandhan, M. K.; Zhang, J.; Ho, P. C.; Mahendran, R.; Zhang, Y. *In Vivo* Photodynamic Therapy Using Upconversion Nanoparticles as Remote-Controlled Nanotransducers. *Nat. Med.* **2012**, *18*, 1580−1585.
(93) Andrew, P. Energy Transfer Across a Metal Film Mediated by Surface Plasmon Polaritons. *Science* **2004**, *306*, 1002−1005.
(94) Blum, C.; Zijlstra, N.; Lagendijk, A.; Wubs, M.; Mosk, A. P.; Subramaniam, V.; Vos, W. L. Nanophotonic Control of the Förster Resonance Energy Transfer Efficiency. *Phys. Rev. Lett.* **2012**, *109*, 203601.
(95) Ghenuche, P.; de Torres, J.; Moparthi, S. B.; Grigoriev, V.; Wenger, J. Nanophotonic Enhancement of the Förster Resonance Energy-Transfer Rate with Single Nanoapertures. *Nano Lett.* **2014**, 4704−4714.

(96) Zhang, X.; Marocico, C. A.; Lunz, M.; Gerard, V. A.; Gun'ko, Y. K.; Lesnyak, V.; Gaponik, N.; Susha, A. S.; Rogach, A. L.; Bradley, A. L. Experimental and Theoretical Investigation of the Distance Dependence of Localized Surface Plasmon Coupled Förster Resonance Energy Transfer. *ACS Nano* **2014**, *8*, 1273−1283.
(97) de Dood, M.; Knoester, J.; Tip, A.; Polman, A. Förster Transfer and the Local Optical Density of States in Erbium-Doped Silica. *Phys. Rev. B* **2005**, *71*, 115102.
(98) Nakamura, T.; Fujii, M.; Miura, S.; Inui, M.; Hayashi, S. Enhancement and Suppression of Energy Transfer from Si Nanocrystals to Er Ions through a Control of the Photonic Mode Density. *Phys. Rev. B* **2006**, *74*, 045302.
(99) Gonzaga-Galeana, J. A.; Zurita-Sánchez, J. R. A Revisitation of the Förster Energy Transfer near a Metallic Spherical Nanoparticle: (1) Efficiency Enhancement or Reduction? (2) The Control of the Förster Radius of the Unbounded Medium. (3) The Impact of the Local Density of States. *J. Chem. Phys.* **2013**, *139*, 244302.
(100) Briggs, J. A.; Atre, A. C.; Dionne, J. A. Narrow-Bandwidth Solar Upconversion: Case Studies of Existing Systems and Generalized Fundamental Limits. *J. Appl. Phys.* **2013**, *113*, 124509.
(101) Feng, W.; Sun, L.-D.; Yan, C.-H. Ag Nanowires Enhanced Upconversion Emission of $NaYF_4$:Yb,Er Nanocrystals *via* a Direct Assembly Method. *Chem. Commun.* **2009**, 4393.
(102) da Silva, D. M.; Kassab, L. R. P.; Lüthi, S. R.; de Araújo, C. B.; Gomes, A. S. L.; Bell, M. J. V. Frequency Upconversion in Er^{3+} Doped $PbO-GeO_2$ Glasses Containing Metallic Nanoparticles. *Appl. Phys. Lett.* **2007**, *90*, 081913.
(103) Li, Z.; Wang, L.; Wang, Z.; Liu, X.; Xiong, Y. Modification of $NaYF_4$:Yb,Er@SiO_2 Nanoparticles with Gold Nanocrystals for Tunable Green-to-Red Upconversion Emissions. *J. Phys. Chem. C* **2011**, *115*, 3291−3296.
(104) Wu, Y.; Shen, X.; Dai, S.; Xu, Y.; Chen, F.; Lin, C.; Xu, T.; Nie, Q. Silver Nanoparticles Enhanced Upconversion Luminescence in Er^{3+}/Yb^{3+} Codoped Bismuth−Germanate Glasses. *J. Phys. Chem. C* **2011**, *115*, 25040−25045.
(105) Paudel, H. P.; Zhong, L.; Bayat, K.; Baroughi, M. F.; Smith, S.; Lin, C.; Jiang, C.; Berry, M. T.; May, P. S. Enhancement of Near-Infrared-to-Visible Upconversion Luminescence Using Engineered Plasmonic Gold Surfaces. *J. Phys. Chem. C* **2011**, *115*, 19028−19036.